EDGE ARTICLE

Check for updates

Molecular nanoribbon gels†

Marta Martínez-Abadía, [ID] [a] Rajeev K. Dubey, [ID] [a] Mercedes Fernández, [ID] [a] Miguel Martín-Arroyo,[a] Robert Aguirresarobe,[a] Akinori Saeki [ID] [b] and Aurelio Mateo-Alonso [ID] *[ac]

Herein, we show that twisted molecular nanoribbons with as many as 322 atoms in the aromatic core are efficient gelators capable of self-assembling into ordered π-gels with morphologies and sol–gel transitions that vary with the length of the nanoribbon. In addition, the nanoribbon gels show a red fluorescence and also pseudoconductivity values in the same range as current state-of-the-art π-gels.
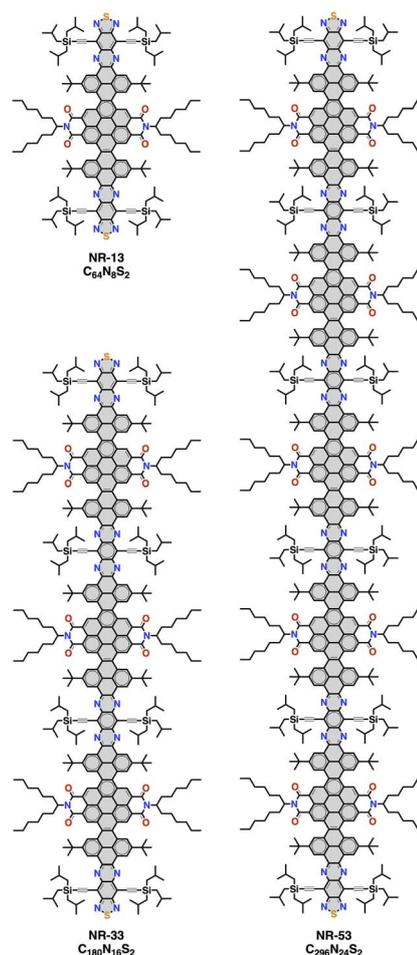
Introduction

π-Gels[1] are the result of the spontaneous aggregation of π-conjugated systems into coiled fibrils. Notably, π-gels offer a combination of properties not found in other organic materials. For example, the spontaneous and reversible organization of π-gels can be used to prepare self-assembled materials for optoelectronic applications.[1a,2] In addition, π-gels can be healed by taking advantage of the reversibility of the sol–gel transition. Also, given their fluidity and their soft nature, π-gels can be processed by liquid deposition methods and can be used to fabricate flexible devices.

Polyclic aromatic hydrocarbons have attracted a lot of attention as gelators[1d–f,2p] since their extended π-surface favours π-stacking, which in turn, enables the formation of optimal channels for electronic and excitonic transport. The use of molecular nanographenes as gelators can potentially increase the performance of π-gels because of their larger π-surfaces. Even if there has been an increasing effort in the synthesis of giant nanographenes with >150 atoms in their aromatic core,[3] current state-of-the-art nanographene gelators are constituted of C_{24} (ref. 4) and C_{68} (ref. 5) cores. This illustrates that incorporation of nanographenes in π-gels is a challenging task, mostly because of the large dimensions and monodisperse nature of nanographenes that favour the typical precipitation/crystallization of the gelator from the gel phase.[1d,e] Another aspect to consider is the planarity of the nanographene core. Although most nanographene gelators are planar,[4] it has been

[a]POLYMAT, University of the Basque Country UPV/EHU, Avenida de Tolosa 72, E-20018 Donostia-San Sebastián, Spain. E-mail: amateo@polymat.eu

[b]Department of Applied Chemistry, Graduate School of Engineering, Osaka University, Suita, Osaka 565-0871, Japan

[c]Ikerbasque, Basque Foundation for Science, Bilbao, Spain

Fig. 1 Chemical structures of **NR-13**, **NR-33** and **NR-53**. The chemical formula corresponds only to the aromatic core atoms highlighted in grey.
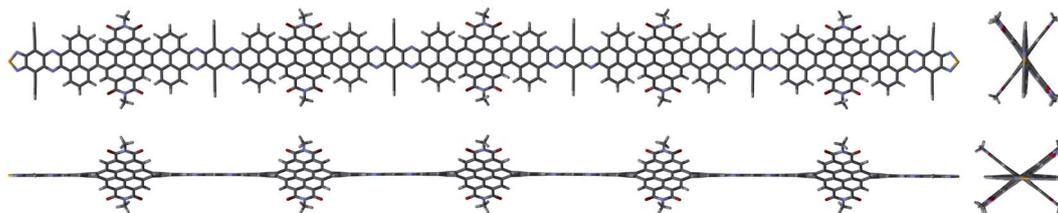
Fig. 2 Different front and side views of a **NR-53** model[3n] without solubilizing groups illustrating its twisted structure.

recently shown that negatively curved nanographenes can also behave as an efficient gelators.[5]

In 2021, some of us reported the synthesis of a family of giant molecular nanoribbons (NRs) with $C_{64}N_8S_2$, $C_{180}N_{16}S_2$ and $C_{296}N_{24}S_2$ cores (respectively, **NR-13**, **NR-33** and **NR-53**, Fig. 1),[3n] constituted by pyrene, coronenebisimide, pyrazinoquinoxaline and quinoxalinothiadiazol units. These NRs combine a selection of solubilizing groups with a twisted aromatic framework that endows them with a high solubility. The NR backbone is twisted 34° at each coronene–pyrene junction as the result of steric congestion between the hydrogens at such cove regions (Fig. 2).

Herein, we show that despite their large dimensions and their twisted structure **NR-13**, **NR-33** and **NR-53** are efficient gelators that are able to self-assemble in 1-octanol at concentrations <3% to produce gels with morphologies that vary with the length of the NR. In addition, the NR π-gels show a red fluorescence and also pseudoconductivity values in the same range as current state-of-the-art π-gels.

Results and discussion

Gelation studies

The gelation and aggregation abilities of **NR-13**, **NR-33** and **NR-53** were studied in 1-butanol, 1-octanol and nitrobenzene. The criterion for the gel formation was the vial inverting method at room temperature by checking whether the sample flows. We found that the three NRs were suitable organogelators in 1-octanol, whereas in nitrobenzene only **NR-13** and **NR-33** were able to form gels. The three NRs produced opaque purple gels in 1-octanol upon cooling to room temperature in air. The gels exhibit reversible sol to gel phase transitions and are stable at room temperature for months. The minimum gelation concentration in 1-octanol for **NR-13** is 3.0% (w/w), while for **NR-33** and **NR-53** is 1.3% (w/w). Below these concentrations, the NRs form aggregates that cannot retain the solvent.

Microscopy

Microscopy investigations reveal that the morphology of the gels depends directly on the length of the NR. The morphology of the dried gels (xerogels) was examined by scanning electron microscopy (SEM). The SEM images acquired from the xerogels of **NR-13** (Fig. 3a and S1†) clearly showed rigid long fibrils, which exhibit lengths up to tens of μm and in some cases even longer. These fibrils show widths ranging from 0.40 to 2.5 μm, but they also vary in height (Fig. S1b†). The aggregates of **NR-13**

in 1-octanol at lower concentration (0.07% w/w), in which the gelation does not take place, were studied by transmission electron microscopy (TEM), showing shorter fibrils but in the same range of width (Fig. 3d). For **NR-33**, the SEM images of the xerogels showed shorter and thinner fibrils (Fig. 3b and S2†) than the ones of **NR-13**. These **NR-33** fibrils are homogeneous in width (200–250 nm) and show lengths of several μm. The same trend was observed by TEM (0.1% w/w), with thin fibrils which possess a length of 1–2 μm and widths of hundreds of nanometers (Fig. 3e). In contrast to the xerogels of **NR-13** and **NR-33**, the SEM images show that the xerogel of **NR-53** is constituted by homogeneous spherical particles of 25–29 nm of diameter

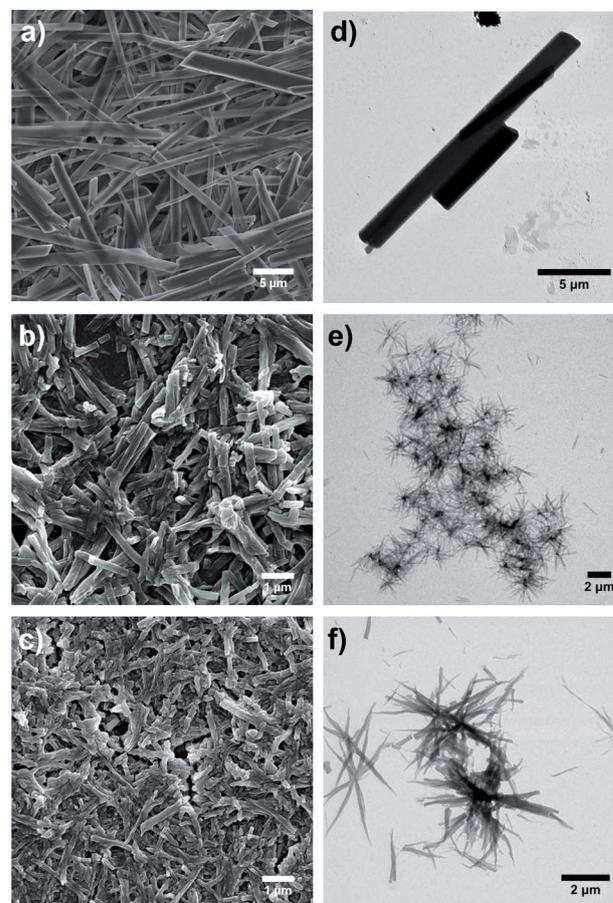**Fig. 3** SEM images of the xerogels, in 1-octanol, of (a) **NR-13** (3% w/w), (b) **NR-33** (1.3% w/w), and (c) **NR-53** (1.3% w/w). TEM images of the aggregates in 1-octanol of (d) **NR-13** (0.07% w/w), (e) **NR-33** (0.1% w/w), and (f) **NR-53** (0.1% w/w).
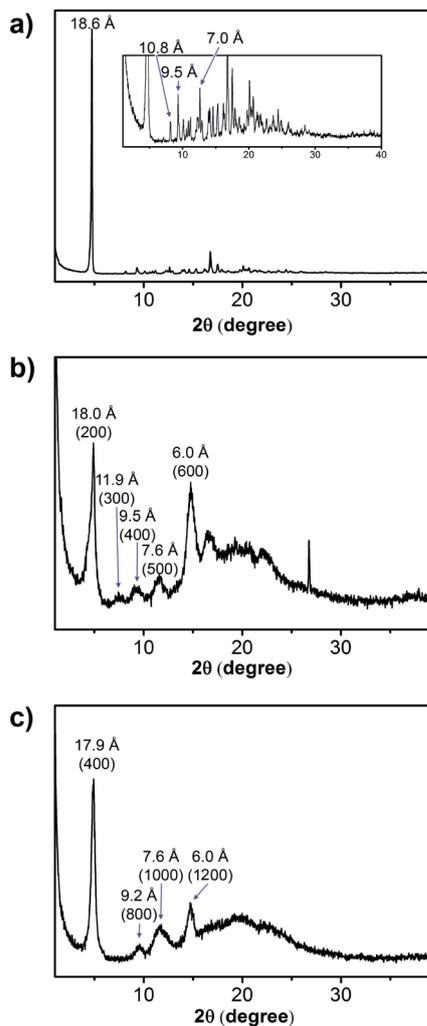
Fig. 4 X-Ray powder diffraction pattern from the xerogels obtained from the 1-octanol gels of (a) **NR-13** (3.0% w/w); (b) **NR-33** (1.3% w/w); and (c) **NR-53** (1.3% w/w).

Fig. 5 Rheological characterization. Frequency sweep test at $T = 20\,^{\circ}C$ of **NR-13** (3% w/w), **NR-33** (1.3% w/w), and **NR-53** (1.3% w/w).

Rheology

Rheological experiments were carried out in order to confirm the gel nature of the samples (Fig. 5). Small Amplitude Oscillatory Shear (SAOS) experiments at 20 °C showed $G' > G''$ values that are frequency-independent, which correspond to a percolated network structure. To investigate the thixotropic behaviour, we subjected the samples to shear rate ramps (increase-steady-decrease). The samples showed a marked pseudoplastic behaviour, but after shearing, the samples do not recover their initial gel-like structure as the viscosity remains constant and low upon shearing as illustrated for **NR-53** (Fig. S4†). This effect, that can be ascribed to the orientation of the nanoribbons in the flow direction, was further investigated by large amplitude oscillatory shear (LAOS) experiments. The results (Fig. S5 and S6†) indicate that the supramolecular assembly loses its elastic property at high strain values, as $G'' > G'$ was observed, indicating the rupture of the gel network. Similarly, continuous step–strain cycles at low (0.5%) and high (100%) strain showed that, once the strain is released, a weak structural rearrangement occurs, as the elastic property is restored again ($G' > G''$), although the moduli were not fully recovered and the sol–gel process was only partially reversed.

The rheological behaviour correlates with the different morphologies of the gels. The thin, flexible fibrils of the **NR-53** gel lead to the formation of a denser and more entangled nanofibrous structure with higher moduli than the stiffer fibers of **NR-33** and **NR-13** gels, which, as expected, result in a network with poorer connectivity. Therefore, the flexibility of the fibers increases the junction number density, improving the macroscopic viscoelastic response. This is consistent with previous observations on pyrene-based supramolecular gels, where the nanoscale flexibility of supramolecular packing was suggested to strongly influence the mechanical strength of the gel.[6]

Sol–gel transition

The sol–gel transitions ($T_{sol–gel}$) of the different gels were estimated by monitoring visually the changes in the fluidity of the samples with the temperature. The measurements illustrate how the $T_{sol–gel}$ of the different gels increase with the increasing length of the NR (48, 61 and 77 °C, respectively for **NR-13**, **NR-33**

(Fig. 3c and S3†) that aggregate forming fibrils of several μm. In the case of **NR-53** (0.1% w/w in 1-octanol), the TEM images revealed a different morphology than the corresponding xerogel. In fact, thin flexible fibrils (Fig. 3f) with widths up to 180 nm and lengths of several μm were observed.

X-ray diffraction

The crystallinity of the xerogels of **NR-13**, **NR-33** and **NR-53** was confirmed by powder X-ray diffraction (PXRD), which showed several intense diffraction peaks with a similar pattern (Fig. 4). The xerogel of **NR-13** exhibits a pattern of sharp signals, indicating a high degree of crystallinity (Fig. 4a), which differs from the single crystal structure reported.[3n] The xerogels of the longer **NR-33** and **NR-53**, show a similar pattern of broader peaks (Fig. 4b and c). In the case of **NR-33** and **NR-53** the d-spacings are consistent a lamellar packing. Indexing in both cases corresponds to those shown in Fig. 4 or to multiples of these. The broadening can be ascribed to the fact that the original gels of the larger nanoribbons were more viscous and retained more solvent.
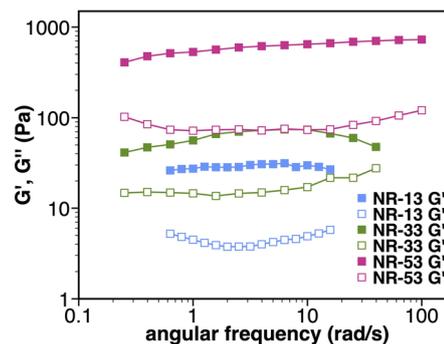
and **NR-53**). Even if there is a clear correlation between NR length and $T_{sol-gel}$, a linear correlation cannot be established because of the different minimum gelation concentration of the gel of **NR-13**.

Optoelectronic properties

Since the gels are opaque, the absorption spectra could not be recorded either in the gel or xerogel state (Fig. 6d–f). Nevertheless, the gels show a red fluorescent emission in all cases upon exposure to UV light. Therefore, the emission spectra of a diluted 1-octanol solution, the sol state, and the xerogel state were recorded and compared (Fig. 6a–c). In 1-octanol solutions, the emission spectra evidence a vibronically-resolved fluorescence band with maxima at 618, 618 and 620 nm respectively for **NR-13**, **NR-33** and **NR-53**, similar to the fluorescence spectra reported in chloroform.[3n] In the sol state (Fig. S7†), the above-mentioned fluorescence emission coexists with a much more intense and red shifted emission band with maxima at 693, 687 and 675 nm,
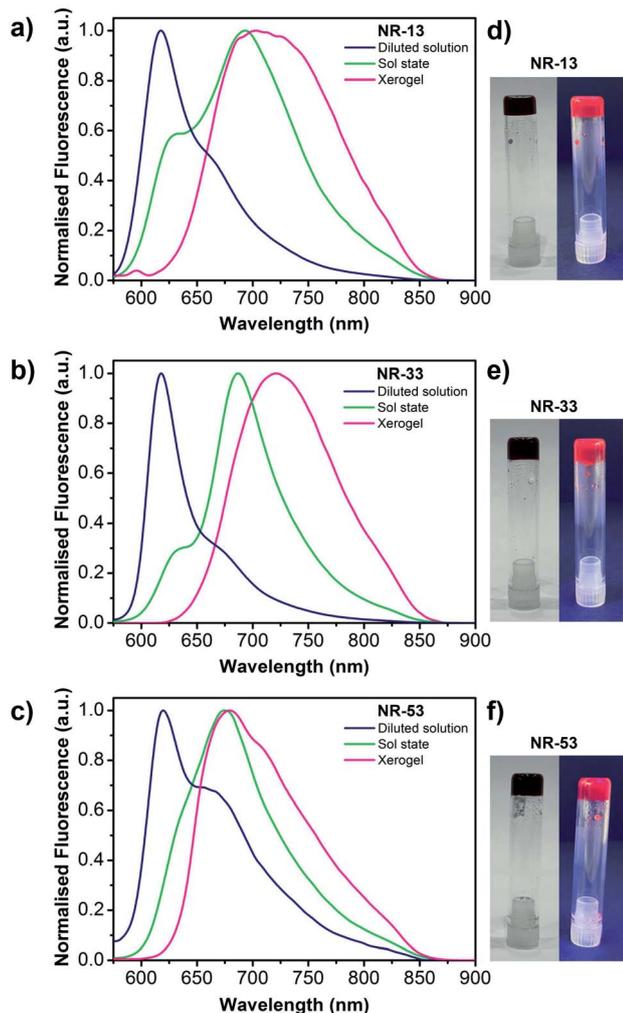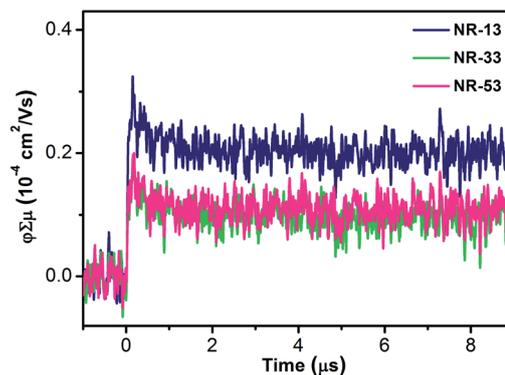

Fig. 7 Conductivity transients of the xerogels of **NR-13**, **NR-33** and **NR-53** upon excitation at 355 nm, 9.1×10^{15} photons per cm^2 per pulse.

respectively for **NR-13**, **NR-33** and **NR-53**, which indicate π-stacking in agreement with previous observations on other nanographene gels with extended cores.[4,5] In the xerogels, also a red shifted featureless band with a similar broadness but with different maxima at 703, 721 and 679 nm, respectively for **NR-13**, **NR-33** and **NR-53**, can be observed, being also consistent with π-stacking.[4,5] Excitation spectra of the xerogels were recorded upon excitation at the fluorescence maxima, showing the same trends observed in the fluorescence measurements (Fig. S8†).

Photoconductivity

The charge transport properties of the NR xerogels were assessed by flash-photolysis time-resolved microwave conductivity (FP-TRMC).[7] FP-TRMC measures the pseudoconductivity ($\varphi\Sigma\mu$, where φ is the product of the quantum yield, and $\Sigma\mu$ is the sum of the charge carrier mobilities) directly from powder samples under an oscillating microwave electric field without the need of metal contacts. The $\varphi\Sigma\mu$ value is directly related to the minimum or inherent charge carrier mobility of the material. The measurements on the xerogels (Fig. 7) show very similar $\varphi\Sigma\mu$ maxima ($\varphi\Sigma\mu_{max}$) for **NR-13** (0.25×10^{-4} cm^2 V^{-1} s^{-1}), **NR-33** (0.14×10^{-4} cm^2 V^{-1} s^{-1}) and **NR-53** (0.14×10^{-4} cm^2 V^{-1} s^{-1}). This $\varphi\Sigma\mu_{max}$ values are in the same range as those of fullerenes,[8] giant molecular nanoribbons,[3e] nanographenes,[3i] and undoped π-gels.[2e,h,p] The half lifetimes ($\tau_{1/2}$) extend beyond the ms in all cases. A likely rationale would be the formation of stable charge separated states that delay charge recombination, in agreement with previous electrochemical and theoretical studies[3n] that illustrate the generation of reversible radical-anions and the localization of two quasidegenerate LUMOs on each of the pyrazinobenzothiadiazole ends of the NRs.

Conclusions

To conclude we have shown that despite their twisted structure and their dimensions, giant molecular NRs can act as optimal gelators that produce ordered π-gels with morphologies that vary with the length of the NRs. Fluorescence spectroscopy evidences the existence of π–π stacking in the gels and also

Fig. 6 Fluorescence spectra of a diluted solution in 1-octanol, sol state and xerogel of (a) **NR-13**; (b) **NR-33**; and (c) **NR-53**. Gelation test in 1-octanol, under room light (left) and UV light (right), of: (d) **NR-13** (3% w/w); (e) **NR-33** (1.3% w/w); and (f) **NR-53** (1.3% w/w).

their red emitting properties. FP-TRMC shows that the NR gels display $\varphi\Sigma\mu$ values in the same range as state-of-the-art giant nanographenes[3e,i] and π-gels.[2e,h,p] Overall, this work opens up new possibilities for the organization of molecular nanoribbons into functional materials and their implementation into organic optoelectronic devices by low-cost and large-area liquid deposition methods.

Author contributions

M. M.-Ab. carried out the gelation experiments, the optical characterization and prepared the samples for SEM and TEM microscopy and for PXRD. R. K. D. carried out the synthesis of the nanoribbons. M. F. and R. A. carried out and interpret the rheology measurements. M. M.-Ar. established the sol–gel transitions. A. S. carried out the FP-TRMC measurements. A. M.-A. conceived and conceptualized the project. M. M.-Ab. and A. M.-A. co-wrote the manuscript. All authors further contributed to the discussion of the experimental work and the final version of the manuscript.

Conflicts of interest

The authors declare no conflict of interest.

Acknowledgements

Notes and references

1 (a) Y. F. Yao, L. Zhang, E. Orgiu and P. Samori, *Adv. Mater.*, 2019, **31**, 1900599; (b) F. Lu, E. A. Neal and T. Nakanishi, *Acc. Chem. Res.*, 2019, **52**, 1834–1843; (c) C. D. Jones and J. W. Steed, *Chem. Soc. Rev.*, 2016, **45**, 6546–6596; (d) S. Ghosh, V. K. Praveen and A. Ajayaghosh, *Annu. Rev. Mater. Res.*, 2016, **46**, 235–262; (e) S. S. Babu, V. K. Praveen and A. Ajayaghosh, *Chem. Rev.*, 2014, **114**, 1973–2129; (f) S. S. Babu, S. Prasanthkumar and A. Ajayaghosh, *Angew. Chem., Int. Ed.*, 2012, **51**, 1766–1776.

2 (a) J.-P. Hong, M.-C. Um, S.-R. Nam, J.-I. Hong and S. Lee, *Chem. Commun.*, 2009, 310–312; (b) Y.-S. Guan, Y. Qin, Y. Sun, J. Chen, W. Xu and D. Zhu, *Chem. Commun.*, 2016, **52**, 4648–4651; (c) A. A. Sagade, K. V. Rao, U. Mogera, S. J. George, A. Datta and G. U. Kulkarni, *Adv. Mater.*, 2013, **25**, 559–564; (d) Y.-S. Guan, Y. Qin, Y. Sun, C. Wang, W. Xu and D. Zhu, *Chem. Commun.*, 2015, **51**, 12182–12184; (e) S. Prasanthkumar, A. Saeki, S. Seki and A. Ajayaghosh, *J. Am. Chem. Soc.*, 2010, **132**, 8866–8867; (f) M. J. Hollamby, M. Karny, P. H. H. Bomans, N. A. J. M. Sommerdjik, A. Saeki, S. Seki, H. Minamikawa, I. Grillo, B. R. Pauw, P. Brown, J. Eastoe, H. Möhwald and T. Nakanishi, *Nat. Chem.*, 2014, **6**, 690; (g) J. López-Andarias, M. J. Rodriguez, C. Atienza, J. L. López, T. Mikie, S. Casado, S. Seki, J. L. Carrascosa and N. Martín, *J. Am. Chem. Soc.*, 2015, **137**, 893–897; (h) V. S. Nair, R. D. Mukhopadhyay, A. Saeki, S. Seki and A. Ajayaghosh, *Sci. Adv.*, 2016, **2**, e1600142; (i) C. Martín, K. Kennes, M. Van der Auweraer, J. Hofkens, G. de Miguel and E. M. García-Frutos, *Adv. Funct. Mater.*, 2017, **27**, 1702176; (j) E. R. Draper, J. J. Walsh, T. O. McDonald, M. A. Zwijnenburg, P. J. Cameron, A. J. Cowan and D. J. Adams, *J. Mater. Chem. C*, 2014, **2**, 5570–5575; (k) W.-W. Tsai, I. D. Tevis, A. S. Tayi, H. Cui and S. I. Stupp, *J. Phys. Chem. B*, 2010, **114**, 14778–14786; (l) D. A. Stone, A. S. Tayi, J. E. Goldberger, L. C. Palmer and S. I. Stupp, *Chem. Commun.*, 2011, **47**, 5702–5704; (m) J. Xu, Y. Wang, H. Shan, Y. Lin, Q. Chen, V. A. L. Roy and Z. Xu, *ACS Appl. Mater. Interfaces*, 2016, **8**, 18991–18997; (n) L. Zhang, S. Li, M. A. Squillaci, X. Zhong, Y. Yao, E. Orgiu and P. Samorì, *J. Am. Chem. Soc.*, 2017, **139**, 14406–14411; (o) K. Besar, H. A. M. Ardoña, J. D. Tovar and H. E. Katz, *ACS Nano*, 2015, **9**, 12401–12409; (p) M. Martinez-Abadia, G. Antonicelli, A. Saeki and A. Mateo-Alonso, *Angew. Chem., Int. Ed.*, 2018, **57**, 8209–8213.

3 (a) X. Guo, Z. Yuan, Y. Zhu, Z. Li, R. Huang, Z. Xia, W. Zhang, Y. Li and J. Wang, *Angew. Chem., Int. Ed.*, 2019, **58**, 16966–16972; (b) Y. Zhu, Z. Xia, Z. Cai, Z. Yuan, N. Jiang, T. Li, Y. Wang, X. Guo, Z. Li, S. Ma, D. Zhong, Y. Li and J. Wang, *J. Am. Chem. Soc.*, 2018, **140**, 4222–4226; (c) S. Ma, J. Gu, C. Lin, Z. Luo, Y. Zhu and J. Wang, *J. Am. Chem. Soc.*, 2020, **142**, 16887–16893; (d) C. M. Cruz, I. R. Márquez, S. Castro-Fernández, J. M. Cuerva, E. Maçôas and A. G. Campaña, *Angew. Chem., Int. Ed.*, 2019, **58**, 8068–8072; (e) D. Cortizo-Lacalle, J. P. Mora-Fuentes, K. Strutyński, A. Saeki, M. Melle-Franco and A. Mateo-Alonso, *Angew. Chem., Int. Ed.*, 2018, **57**, 703–708; (f) X. Yan, X. Cui and L.-s. Li, *J. Am. Chem. Soc.*, 2010, **132**, 5944–5945; (g) Y. Chen, C. Lin, Z. Luo, Z. Yin, H. Shi, Y. Zhu and J. Wang, *Angew. Chem., Int. Ed.*, 2021, **60**, 7796–7801; (h) Y. Wang, Z. Yin, Y. Zhu, J. Gu, Y. Li and J. Wang, *Angew. Chem., Int. Ed.*, 2019, **58**, 587–591; (i) J. P. Mora-Fuentes, A. Riaño, D. Cortizo-Lacalle, A. Saeki, M. Melle-Franco and A. Mateo-Alonso, *Angew. Chem., Int. Ed.*, 2019, **58**, 552–556; (j) U. Beser, M. Kastler, A. Maghsoumi, M. Wagner, C. Castiglioni, M. Tommasini, A. Narita, X. Feng and K. Müllen, *J. Am. Chem. Soc.*, 2016, **138**, 4322–4325; (k) C. D. Simpson, J. D. Brand, A. J. Berresheim, L. Przybilla, H. J. Räder and K. Müllen,

Chem.–Eur. J., 2002, **8**, 1424–1429; (*l*) Y.-Z. Tan, B. Yang, K. Parvez, A. Narita, S. Osella, D. Beljonne, X. Feng and K. Müllen, *Nat. Commun.*, 2013, **4**, 2646; (*m*) Y. Zhu, X. Guo, Y. Li and J. Wang, *J. Am. Chem. Soc.*, 2019, **141**, 5511–5517; (*n*) R. K. Dubey, M. Melle-Franco and A. Mateo-Alonso, *J. Am. Chem. Soc.*, 2021, **143**, 6593–6600; (*o*) F. Hernández-Culebras, M. Melle-Franco and A. Mateo-Alonso, *Angew. Chem., Int. Ed.*, 2022, e202205018.

4 (*a*) S. Ito, P. T. Herwig, T. Böhme, J. P. Rabe, W. Rettig and K. Müllen, *J. Am. Chem. Soc.*, 2000, **122**, 7698–7706; (*b*) L. Zhi, J. Wu and K. Müllen, *Org. Lett.*, 2005, **7**, 5761–5764; (*c*) H.-S. Kim, J.-H. Lee, T.-H. Kim, S. Okabe, M. Shibayama and S.-M. Choi, *J. Phys. Chem. B*, 2011, **115**, 7314–7320; (*d*) X. Dou, W. Pisula, J. Wu, G. J. Bodwell and K. Müllen, *Chem.–Eur. J.*, 2008, **14**, 240–249; (*e*) J. P. Hill, W. Jin, A. Kosaka, T. Fukushima, H. Ichihara, T. Shimomura, K. Ito, T. Hashizume, N. Ishii and T. Aida, *Science*, 2004, **304**, 1481–1483; (*f*) W. Jin, T. Fukushima, M. Niki, A. Kosaka, N. Ishii and T. Aida, *Proc. Natl. Acad. Sci. U.S.A.*, 2005, **102**, 10801–10806; (*g*) W. Jin, Y. Yamamoto, T. Fukushima, N. Ishii, J. Kim, K. Kato, M. Takata and T. Aida, *J. Am. Chem. Soc.*, 2008, **130**, 9434–9440; (*h*) K. V. Rao, K. Jayaramulu, T. K. Maji and S. J. George, *Angew. Chem., Int. Ed.*, 2010, **49**, 4218–4222; (*i*) K. V. Rao, K. K. R. Datta, M. Eswaramoorthy and S. J. George, *Angew. Chem., Int. Ed.*, 2011, **50**, 1179–1184; (*j*) A. Jain, K. V. Rao, C. Kulkarni, A. George and S. J. George, *Chem. Commun.*, 2012, **48**, 1467–1469.

5 K. Kato, K. Takaba, S. Maki-Yonekura, N. Mitoma, Y. Nakanishi, T. Nishihara, T. Hatakeyama, T. Kawada, Y. Hijikata, J. Pirillo, L. T. Scott, K. Yonekura, Y. Segawa and K. Itami, *J. Am. Chem. Soc.*, 2021, **143**, 5465–5469.

6 K. Y. Kim, M. Ok, J. Kim, S. H. Jung, M. L. Seo and J. H. Jung, *Gels*, 2020, **6**, 16.

7 A. Saeki, Y. Koizumi, T. Aida and S. Seki, *Acc. Chem. Res.*, 2012, **45**, 1193–1202.

8 S. Reboredo, R. M. Girón, S. Filippone, T. Mikie, T. Sakurai, S. Seki and N. Martín, *Chem.–Eur. J.*, 2016, **22**, 13627–13631.